Journal of Power Sources 196 (2011) 386–392

Contents lists available at ScienceDirect

Journal of Power Sources

journal homepage: www.elsevier.com/locate/jpowsour

Synthesis and characterization of $Li_2Fe_{0.97}M_{0.03}SiO_4$ ($M = Zn^{2+}$, Cu^{2+}, Ni^{2+}) cathode materials for lithium ion batteries

C. Deng [a,*], S. Zhang [b,**], S.Y. Yang [b], B.L. Fu [b], L. Ma [a]

[a] College of Chemistry and Chemical Engineering, Provincial Key Lab for Nano-Functionalized Materials and Excitated States, Harbin Normal University, Harbin 150025, Heilongjiang, China
[b] College of Material Science and Chemical Engineering, Harbin Engineering University, Harbin 150001, Heilongjiang, China

ARTICLE INFO

Article history:
Received 18 December 2009
Received in revised form 11 June 2010
Accepted 21 June 2010
Available online 26 June 2010

Keywords:
Lithium iron orthosilicate
Lithium ion battery
Cation doping
Electrochemical reversibility

ABSTRACT

Attempts to dope Zn^{2+}, Cu^{2+} or Ni^{2+} are made for Li_2FeSiO_4. The effects of dopant on the physical and electrochemical characteristics of Li_2FeSiO_4 were investigated. Zn^{2+} successfully entered into the lattice of Li_2FeSiO_4 and induced the change of lattice parameters. Compared with the undoped Li_2FeSiO_4, $Li_2Fe_{0.97}Zn_{0.03}SiO_4$ has higher discharge capacity, better electrochemical reversibility and lower electrode polarization. The improved electrochemical performance of $Li_2Fe_{0.97}Zn_{0.03}SiO_4$ can be attributed to the improved structural stability and the enhanced lithium ion diffusivity brought about by Zn^{2+} doping. However, Ni^{2+} and Cu^{2+} cannot be doped into the lattice of Li_2FeSiO_4. Cu and NiO are formed as impurities in the Cu- and Ni-containing samples, respectively. Compared with the undoped Li_2FeSiO_4, the Cu- and Ni-containing samples have lower capacities and higher electrochemical polarization.

1. Introduction

The need for large-scale batteries impels the development of new materials for lithium ion batteries. Among the cathode materials under development, polyanion compounds have been recognized as one of the most promising candidate due to its low cost and high safety [1–3]. As a branch of polyanion compounds, lithium transition metal orthosilicates have been synthesized and characterized as cathode materials for lithium ion batteries [4–13]. As shown by the reports of Nyten et al. [14–16], Li_2FeSiO_4 has good electrochemical activity and high cycling stability. However, the poor rate capability of Li_2FeSiO_4, which results from its poor electronic conductivity and lithium ion mobility, inhibits its further use in commercial applications [17,18].

The improvements on electronic conductivity or lithium ion mobility can be achieved in three ways: (1) conductive carbon coating [19]; (2) particle size reduction [20]; (3) supervalent or isovalent cation doping [21]. Individually and in combination, these methods have been used to improve the electrochemical performance of Li_2FeSiO_4. Dominko et al. studied the impact of synthesis conditions on the electrochemical performance of Li_2FeSiO_4. Their results indicate that carbon coating and particle size reduction can effectively improve the electrochemical performance of Li_2FeSiO_4 [22]. Gong et al. prepared carbon-coated nanostructured Li_2FeSiO_4 via hydrothermal method. This material has a discharge capacity as high as 160 mAh g^{-1} at a current density of $C/16$, and it also shows superior high rate capability [23]. Supervalent or isovalent cation doping is often employed to improve the electrochemical performance of polyanion compounds [24,25]. Various cations have been used to dope $LiFePO_4$, and some positive impacts are reported on electrochemical performance [26–28]. Up to the present, attempts to dope isovalent Mn^{2+} and Ni^{2+} have been made to improve the electrochemical performance of Li_2FeSiO_4 [17,29,30]. Gong et al. are the first to report the synthesis and characterization of $Li_2Mn_xFe_{1-x}SiO_4$ ($0 \le x \le 1$) [29]. Beyond one electron reaction can be realized by Mn^{2+} substitution [17], since Mn^{2+} (Ni^{2+}, Co^{2+}) can go from 2+ to 4+. When Fe^{2+} is substituted by these divalent cations, the possibility of a more than one electron reaction is a function of the redox properties of the substituent divalent cation. Recently, Guo et al. prepared and characterized $Li_2Fe_{1-x}Ni_xSiO_4$ ($0 \le x \le 0.3$) as cathode materials for lithium ion batteries, and the improved electrochemical performance is obtained when x is equal to 0.1 [30].

It is believed that there still exists an unexplored reservoir of cation doping which has positive effect on the structural and electrochemical properties of Li_2FeSiO_4. Li_2ZnSiO_4 can be crystallized in space group $Pmn2_1$ (orthorhombic) [31,32]. Moreover, Li_2ZnSiO_4 is a Li ion conductor with high ionic conductivity [33]. Therefore, it is interesting to investigate the doping effect of Zn on the structural and electrochemical characteristics of Li_2FeSiO_4. In addition, the

* Corresponding author. Tel.: +86 451 88060570; fax: +86 451 88060570.
** Corresponding author. Tel.: +86 451 82589186.
E-mail addresses: chaodeng2008@yahoo.cn (C. Deng), senzhang@hrbeu.edu.cn (S. Zhang).

0378-7753/$ – see front matter © 2010 Elsevier B.V. All rights reserved.
doi:10.1016/j.jpowsour.2010.06.064

radius of Cu^{2+} or Ni^{2+} is similar to that of Fe^{2+} [34,35], thus it may be possible to dope Li_2FeSiO_4 with Cu^{2+} or Ni^{2+}. In the $Li_2Fe_{1-x}M_xSiO_4$ system, the increase of x is always accompanied by the decrease of $1-x$, in other words, increasing the amount of M^{2+} will decrease the amount of Fe^{2+}. When M^{2+} (e.g. Zn^{2+}) is not involved in the charge–discharge process, the capacity will decrease with increasing x. Therefore, a small value of 3% is chosen for x in this study.

In this study, we investigated the impact of divalent cation doping on the physical and electrochemical characteristics of Li_2FeSiO_4. It was attempted to dope three divalent cations, i.e. Zn^{2+}, Cu^{2+} and Ni^{2+}, into Li_2FeSiO_4. All the samples were prepared by a sol–gel method, and they were characterized and compared in detail.

2. Experimental

2.1. Synthesis of $Li_2Fe_{0.97}M_{0.03}SiO_4$

$Li_2Fe_{0.97}Zn_{0.03}SiO_4$ was prepared by a sol–gel method based on citric acid as described in our previous report [36]. Stoichiometric amount of analytical reagents, lithium acetate hydrate, ferric citrate, zinc acetate, tetraethyl orthosilicate, and citric acid were used as starting materials. Lithium acetate hydrate, ferric citrate and zinc acetate were first dissolved in distilled water. A saturated aqueous solution of citric acid was slowly added to the above solution under magnetic stirring. After a homogeneous solution is formed, it was transferred into a reflux system where an ethanol solution of tetraethyl orthosilicate is also added. Under magnetic stirring, the reflux was carried out at 80 °C for at least 12 h until a clear greenish solution is formed. The solution was taken out, and then it was kept at 75 °C under magnetic stirring to evaporate ethanol and water. The resulting wet gel was dried in a vacuum oven at 100 °C. The dry gel was ground and then calcined at 700 °C for 12 h in flowing argon. Instead of zinc acetate, copper acetate and nickel acetate were used as the starting materials for Cu and Ni contained samples respectively.

2.2. Measurements

Powder X-ray diffraction (XRD, Bruker D8/Germany) employing Cu $K\alpha_1$ radiation (λ = 1.5406 Å) was used to identify the crystalline phase of the material. The surface morphology was observed with a scanning electron microscope (SEM, HITACHI S-4700), and the chemical composition was determined by an energy dispersive X-ray detector (EDX) coupled with the scanning electron microscope and an atomic absorption spectrometer (AAS, PE Analyst 100). The carbon content was determined from thermogravimetric analysis (TGA, NETZSCH STA 449C). The sample was heated from 35 °C to 800 °C in air at a rate of 10 °C min^{-1}. The carbon content of all the samples is about 10 wt%.

The coin cells were prepared as described in Ref. [36]. The composite electrode was made from a mixture of the prepared sample, acetylene black, and polyvinylidene fluoride in a weight ratio of 80:10:10. Galvanostatic charge–discharge measurements were performed in a potential ranges of 1.5–4.6 V, 2.0–4.6 V and 2.0–3.7 V. The electrochemical impedance measurements were carried out with a CHI 660C instrument. All the electrochemical measurements were carried out at ambient temperature, and the carbon content is corrected in the calculation of capacity.

3. Results and discussion

3.1. Sample characterization

Fig. 1 shows the XRD patterns of all the samples. The XRD pattern of the Zn doped sample is similar to that of the undoped Li_2FeSiO_4.

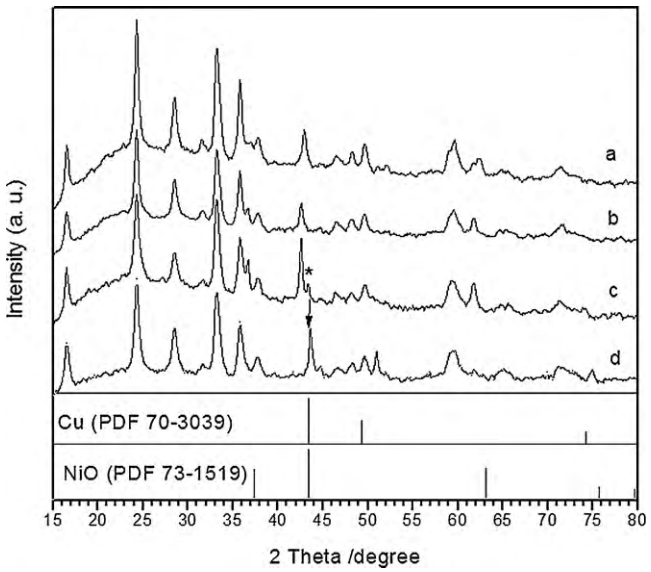

Fig. 1. XRD patterns of the undoped (a), Zn doped (b), Cu- (c) and Ni-containing (d) Li_2FeSiO_4 samples. The stick pattern of Cu (PDF#70-3039) and NiO (PDF#73-1519) are also shown as references.

However, there is clear difference between the XRD pattern of the Ni- or Cu-containing sample and that of the undoped Li_2FeSiO_4. For the Ni-containing sample, the large peak at 43.60° (marked with arrow) can be attributed to NiO (PDF73-1519). For the Cu-containing sample, the small peak at 43.30° (marked with asterisk) can be attributed to Cu (PDF70-3039).

Rietveld refinements were carried out for all the samples and the obtained lattice parameters are listed in Table 1. The refinement result with the observed, calculated and difference profiles of the Zn doped sample are shown in Fig. 2. The lattice parameters of the Ni- and Cu-containing samples are almost the same as those of the undoped Li_2FeSiO_4, and the differences are within error range. The lattice structure of Li_2FeSiO_4 is therefore not changed by the addition of Ni^{2+} or Cu^{2+}. We can deduce that the added Ni^{2+} and Cu^{2+} form impurities rather than dope into the lattice of Li_2FeSiO_4. Compared with the undoped Li_2FeSiO_4, a decrease in all the lattice parameters is observed for the Zn doped sample, which indicates that Zn^{2+} is doped into the lattice of Li_2FeSiO_4.

3.2. SEM observation

The SEM images of all the samples are shown in Fig. 3. All the samples are composed of agglomerated small particles which size is about 100 nm. EDX analysis is carried out to measure the stoichiometry of the Zn doped, Cu- and Ni-containing samples, and the results are shown in Fig. 4. For each sample, a larger region (marked as A) was selected to measure the average composition, and a smaller region (marked as B) was selected to show whether the composition of A is homogeneous on a relatively small scale. The atomic ratios are calculated and listed in Table 2. For the Zn doped sample, the atomic ratios in both region A and region B are similar, and the measured value is close to the designed one. For

Table 1
Lattice parameters of the undoped (a), Zn doped (b), Cu- (c) and Ni- containing (d) Li_2FeSiO_4 samples.

Sample	a (Å)	b (Å)	c (Å)
a	6.2510 ± 0.0017	5.3474 ± 0.0017	5.0102 ± 0.0012
b	6.2340 ± 0.0022	5.3259 ± 0.0030	4.9995 ± 0.0020
c	6.2561 ± 0.0018	5.3472 ± 0.0024	5.0083 ± 0.0013
d	6.2523 ± 0.0027	5.3517 ± 0.0025	5.0106 ± 0.0022

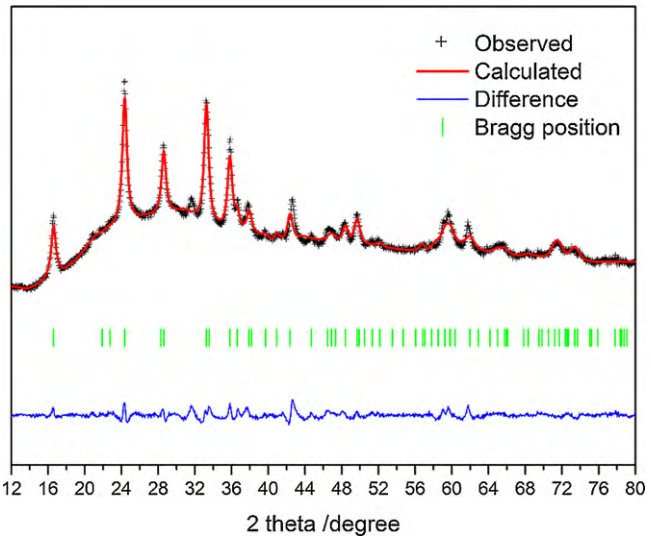

Fig. 2. Refinement result of Zn doped sample with the observed, calculated and difference profiles.

Table 2
Atomic ratios of Zn doped (a), Cu- (b), and Ni-containing (c) samples.

Sample	Atom ratio					
	Region A			Region B		
	Dopant	Fe	Si	Dopant	Fe	Si
a	0.029(Zn)	0.974	1	0.028(Zn)	0.967	1
b	0.034(Cu)	0.965	1	0.018(Cu)	0.974	1
c	0.027(Ni)	0.968	1	0.041(Ni)	0.963	1

the Cu- (or Ni-containing) sample, the atomic ratio in region A is clearly different from the atomic ratio in region B. In the larger region A, the measured atomic ratio is close to the designed value. However, clearly higher or lower amount of Cu (or Ni) is detected in the smaller region B. The non-homogeneous distribution of Cu (or Ni) in the Cu- (or Ni-containing) sample can be attributed to the presence of Cu (or NiO), because impurity can hardly be distributed homogeneously in a relatively small region.

3.3. Electrochemical performance

The initial five charge/discharge curves of all the samples are shown in Fig. 5. The charge and discharge are all conducted at a current density of 10 mA g^{-1}. In order to obtain the full charge/discharge behavior of the samples, a wide potential range of 1.5–4.6 V (vs. Li^+/Li) is used in the initial cycles. For all the samples, the charge potential in the first cycle is higher than those in the subsequent cycles. All the samples show relative large oxidation capacity in the first cycle at potentials above 4 V. Based on the knowledge from some other works [16], this capacity at high voltage is not connected with redox couple Fe^{II}/Fe^{III}. It is likely connected with the oxidation of electrolyte components. The plateau slightly above 3 V can be attributed to the phase transition process [14,15]. For all the samples, these plateaux are short, which suggests that the samples were oxidized during preparation of the composite with PVdF and CB. The longer plateau for the Zn doped sample suggests that this sample has higher amount of Fe^{2+} regarding to the undoped sample.

Compared with the undoped Li_2FeSiO_4, the Zn doped sample shows 2.6% higher discharge capacity. This percentage (2.6%) is close to the percentage of Zn doping (3%). However, the Cu- and Ni-containing samples show 2.9% and 6.6% lower discharge capacities than the undoped Li_2FeSiO_4. The percentage of 2.9% is very close to the Cu^{2+} substitution percentage (3%) for the Cu-containing sample, but the percentage of 6.6% is much higher than the Ni^{2+} substitution percentage (3%) for the Ni-containing sample. These results can be attributed to the fact that Zn^{2+} is successfully incorporated into the structure of Li_2FeSiO_4, while Cu^{2+} and Ni^{2+} form impurities.

As cathode materials for lithium ion batteries, the capacity below 2 V is often useless. Therefore, the cut-off potential of dis-

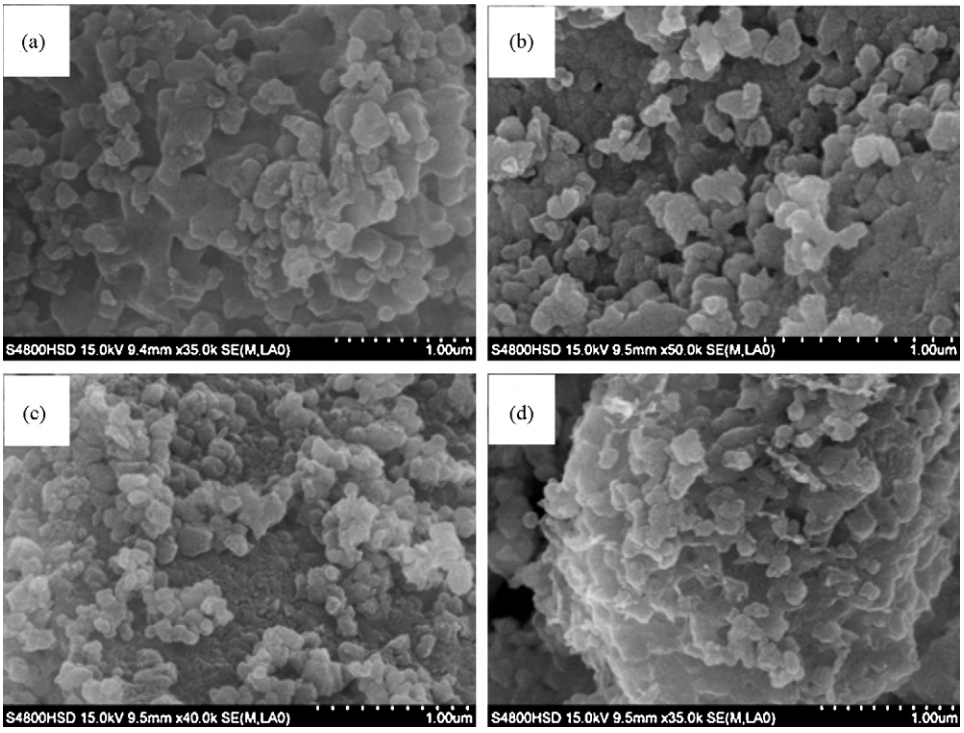

Fig. 3. SEM images of the undoped (a), Zn doped (b), Cu- (c) and Ni-containing (d) Li_2FeSiO_4 samples.

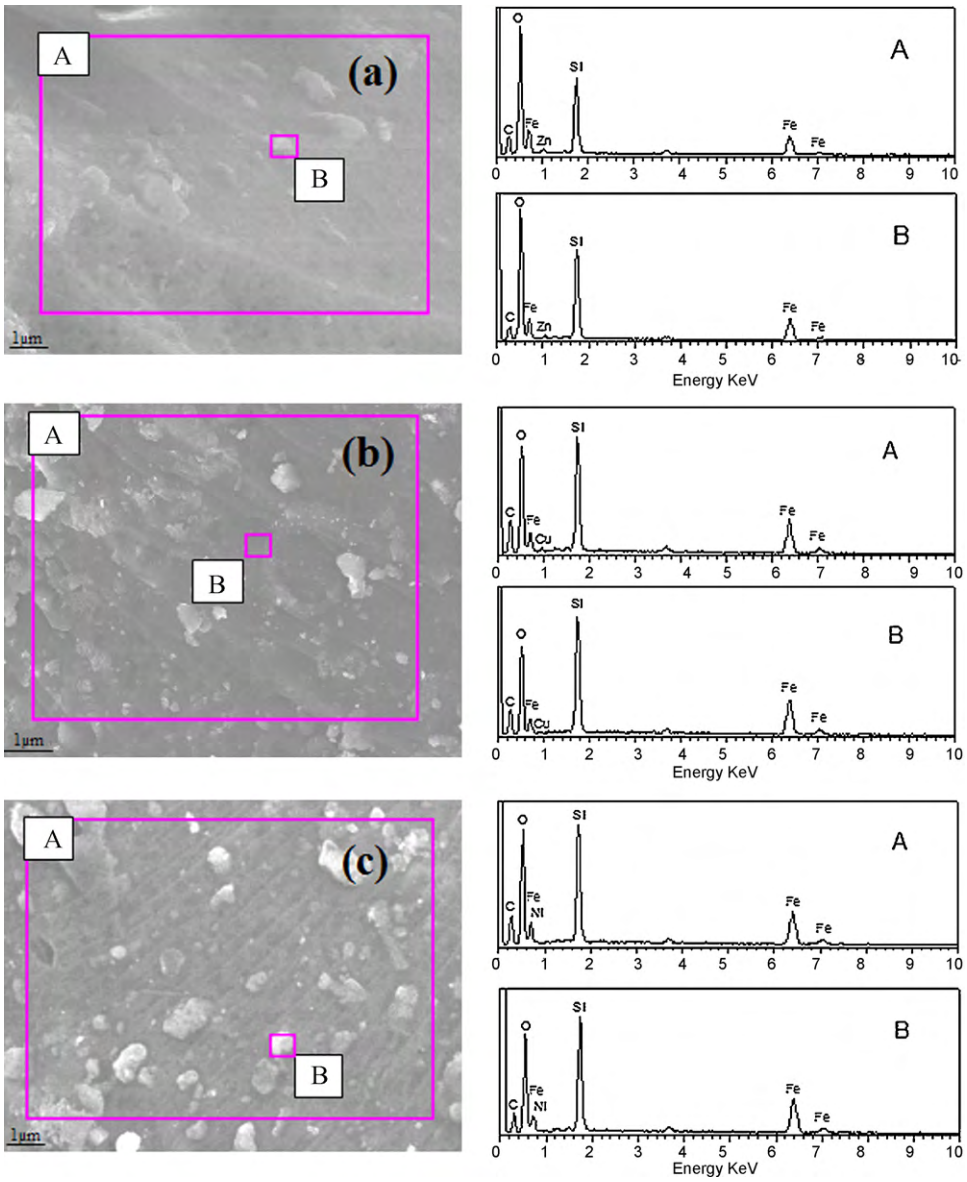

Fig. 4. EDX analysis results of the Zn doped (a), Cu- (b) and Ni-containing (c) samples.

charge is shift to 2 V, and the charge–discharge curves of all the samples are measured. The current density of 10 mA g^{-1} is applied and the results are shown in Fig. 6. In comparison with the capacity down to 1.5 V, the capacities down to 2 V decrease and show similar trend between samples. The discharge capacity of the undoped, Zn doped, Cu- and Ni-containing samples are 128 mAh g^{-1}, 133 mAh g^{-1}, 104 mAh g^{-1} and 86 mAh g^{-1} respectively. The discharge capacity of the Zn doped sample is 3.9% higher than that of the undoped sample. This percentage (3.9%) is close to the percentage of Zn doping (3%). As discussed above, Zn^{2+} is doped into the structure of Li_2FeSiO_4. The improved capacity of the Zn doped sample can be attributed to the stability effect of Zn doping which facilitates the diffusion of lithium ion.

Fig. 7 shows the discharge capacities of all the samples at various current densities, i.e. *C*/10, *C*/3, *C*/2 and 1*C*, in the voltage range of 2–4.6 V (vs. Li^+/Li). As the current density increases, the differences between the samples become more and more pronounced. At the current density of 1*C*, the discharge capacity of the Zn doped sample (92 mAh g^{-1}), is obviously higher than that of the undoped Li_2FeSiO_4 (81 mAh g^{-1}), while the discharge capacities of Cu-containing (60 mAh g^{-1}) and Ni-containing (41 mAh g^{-1}) samples are much lower than that of the undoped Li_2FeSiO_4.

Fig. 8 shows the cycling performance of the Zn doped and undoped Li_2FeSiO_4 at the 1/10*C* and 1*C* rates in the voltage range of 2–4.6 V (Fig. 8(a)) and 2–3.7 V (Fig. 8(b)). In the voltage range of 2–4.6 V, the capacity retentions of the Zn doped and undoped samples are 97.5% and 96.2% at the *C*/10 rate, and 94.8% and 90.6% at the 1*C* rate. In order to alleviate the effect of the electrolyte oxidation, both the Zn doped and undoped samples are also cycled between 2 V and 3.7 V. In the voltage range of 2–3.7 V, the capacity retentions of the Zn doped and undoped samples are 98.7% and 97.6% at the *C*/10 rate, and 96.2% and 92.7% at the 1*C* rate. When the same current density is applied to both the Zn doped and undoped samples, the capacity retentions in the voltage range of 2–3.7 V are higher than those in the voltage range of 2–4.6 V for each sample, which indicates that both samples are more stable in the voltage range of 2–3.7 V. When the same voltage range and current density are used, the capacity retention of the Zn doped sample is

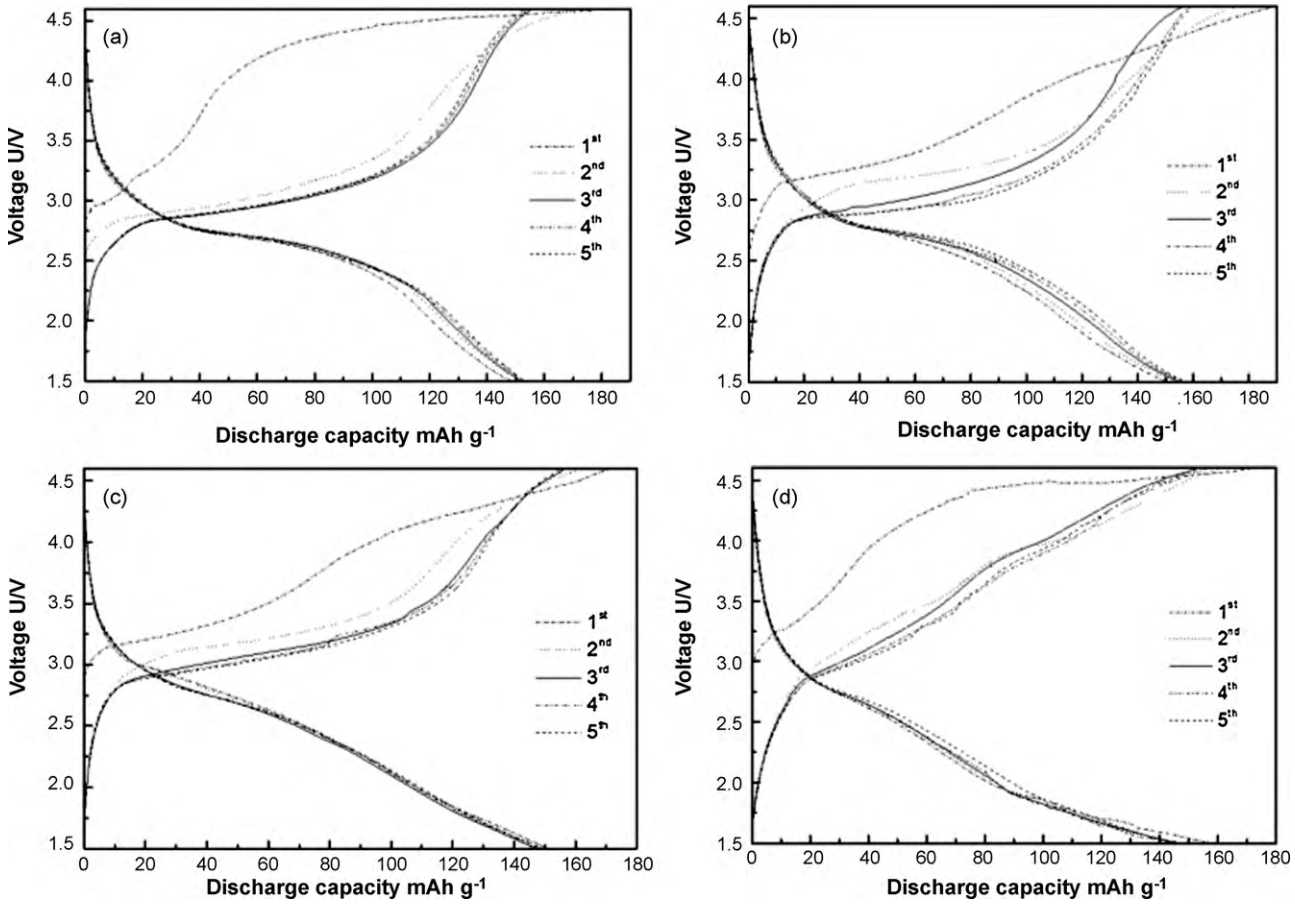

Fig. 5. The initial five charge/discharge curves of the undoped (a), Zn doped (b), Cu- (c) and Ni-containing (d) Li_2FeSiO_4 samples. The voltage range is 1.5–4.6 V.

higher than that of the undoped sample, which indicates the higher cycling stability of the Zn doped sample. The higher cycling stability of the Zn doped sample can be attributed to the effect of Zn doping. During the de/intercalation process, Fe^{2+} is oxidized to Fe^{3+} (Fe^{3+} is reduced to Fe^{2+}), and the crystal lattice of Li_2FeSiO_4 shrinks/expands. Zn^{2+} is not involved in the oxidation/reduction reaction, thus it can stabilize the crystal lattice and improve the cycling stability of Li_2FeSiO_4.

3.4. Electrochemical voltage spectroscopy (EVS) analysis

Electrochemical voltage spectroscopy (EVS) analysis was conducted to study the effect of divalent cation doping and the results are shown in Fig. 9. The redox peaks in the dQ/dV curve correspond to the charge/discharge plateaus in the galvanostatic charge–discharge curve [37]. All the samples have a pair of redox peaks (at about 2.7–2.9 V) in the dQ/dV curves, which can be

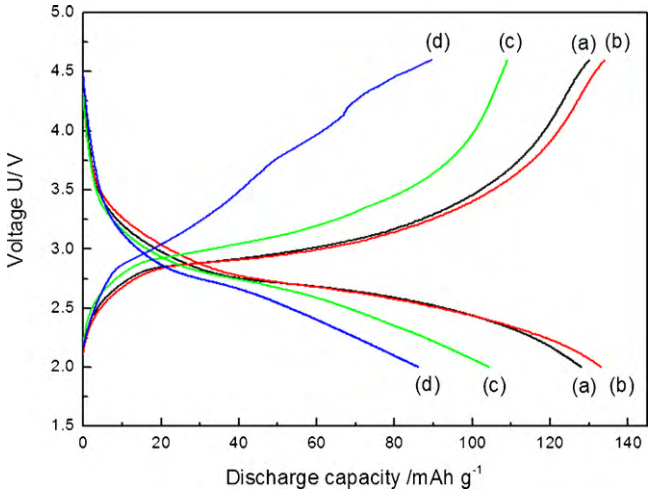

Fig. 6. The charge/discharge curves of the undoped (a), Zn doped (b), Cu- (c) and Ni-containing (d) Li_2FeSiO_4 samples. The voltage range is 2–4.6 V.

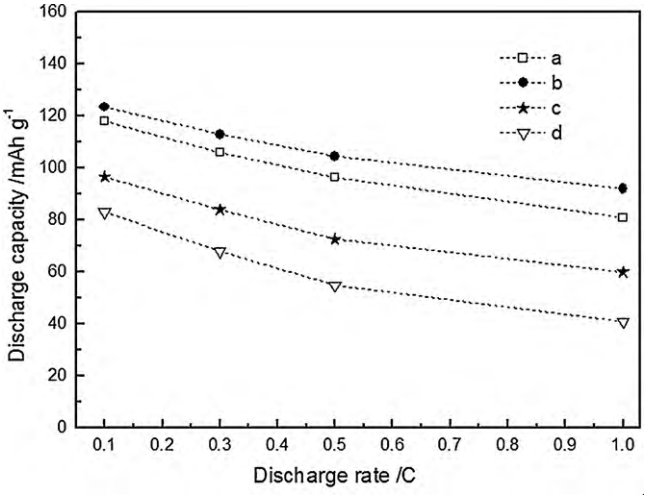

Fig. 7. Discharge capacities of the undoped (a), Zn doped (b), Cu- (c) and Ni-containing (d) Li_2FeSiO_4 samples at various current densities, i.e. $C/10$, $C/3$, $C/2$ and 1C, in the voltage range of 2–4.6 V.

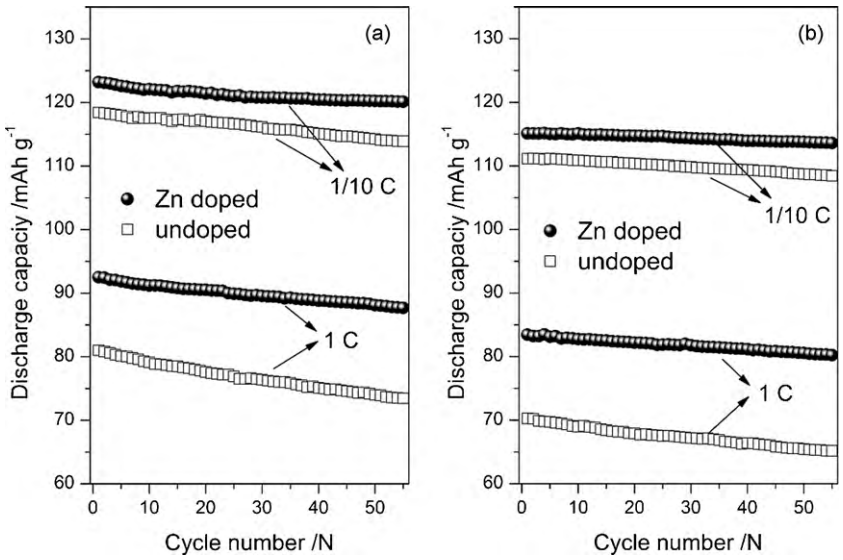

Fig. 8. Cycling performance of the Zn doped and undoped Li_2FeSiO_4 at the 1/10*C* and 1*C* rates in the voltage range of (a) 2–4.6 V and (b) 2–3.7 V (vs. Li^+/Li).

attributed to the redox reaction of Fe^{2+}/Fe^{3+} couple. The potential difference between the oxidation peak and the reduction peak is often used to differentiate the electrochemical reversibility of electrode materials. The lower potential difference is an indication of higher electrochemical reversibility [38]. The potential differences of all the samples are calculated and the results are shown as an inset of Fig. 9. The potential difference of the Zn doped sample is lower than that of the undoped Li_2FeSiO_4, which indicates the higher electrochemical reversibility of the Zn doped sample. However, Cu- and Ni-containing samples exhibit much higher potential differences than undoped Li_2FeSiO_4, which verify their poor electrochemical reversibility.

According to the results of structural and electrochemical characterization, the poor electrochemical performance of the Cu- or Ni-containing sample can be attributed to the existence of impurity, i.e. Cu or NiO. However, it is not the case for the Zn doped sample. Generally, the electrochemical performance of polyanion compounds is limited by their low electronic conductivity and poor ionic conductivity. All the samples contain residual carbon which acts as an electronic conductor and creates an electronic conductive path between particles. Therefore, the electronic conductivity is not the key factor controlling the electrochemical performance of these carbon containing samples. To clarify the origin of the improved electrochemical performance of the Zn doped sample, electrochemical impedance spectroscopy (EIS) measurements were carried out to measure the lithium ion diffusion coefficients of the Zn doped and undoped samples.

3.5. EIS measurements

Fig. 10 shows the Nyquist plots of the Zn doped sample and the undoped sample at fully discharge state. Based on the model reported by Gaberscek et al. [39], the semicircle at high frequency is due to the contact impedance between the electrode materials and current collectors. The sloping line at low frequency can be attributed to the lithium diffusion in solid phase. Both electrodes are prepared in the same way to obtain similar contacts between particles. Before impedance measurements are conducted, the electrodes are fully discharged to ensure that they are saturated with lithium. The lithium diffusion coefficients of both samples are calculated from the low frequency sloping line [40]. The relationship between the Z' and the reciprocal square root of frequency in the

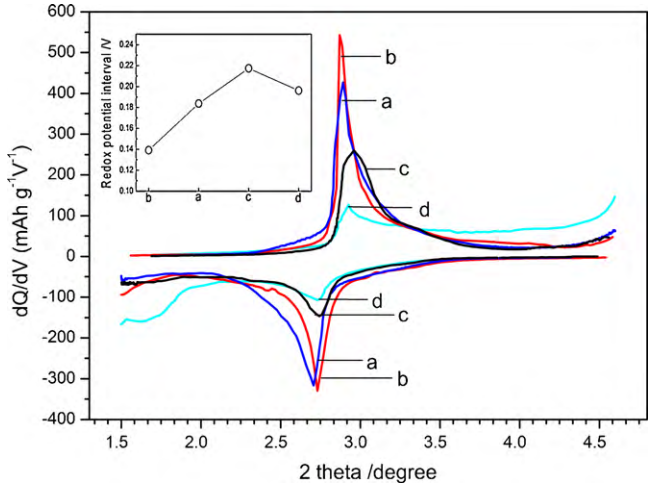

Fig. 9. Differential capacity vs. potential curves of the undoped (a), Zn doped (b), Cu- (c) and Ni-containing (d) Li_2FeSiO_4 samples. The potential difference between the oxidation peak and the reduction peak is shown as an inset.

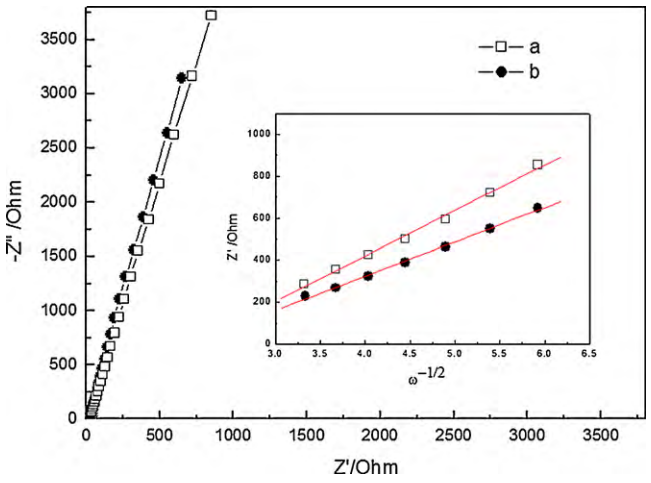

Fig. 10. Nyquist plots of the synthesized undoped (a) and Zn doped (b) Li_2FeSiO_4 samples. The relationship between the Z' and the reciprocal square root of frequency in the low frequency region is shown as an inset.

low frequency region are shown as an inert of Fig. 9. The calculated lithium diffusion coefficients are 4.76×10^{-14} cm^2 s^{-1} and 8.62×10^{-14} cm^2 s^{-1} for undoped and Zn doped samples respectively.

The improved lithium diffusivity of the Zn doped sample can partially be attributed to the improved stability brought about by Zn doping. Zn^{2+} is not oxidized/reduced during the charge/discharge process, thus it can lessen the change of the crystal lattice. This stabilization effect can protect the diffusion path of lithium ion from being distorted and improve the lithium diffusivity. In addition, Li_2ZnSiO_4 has a high ionic conductivity, and it can also be crystallized in the space group of *Pmn2$_1$* (the same as Li_2FeSiO_4). Therefore, Zn doping can improve the lithium diffusivity of Li_2FeSiO_4 and results in better electrochemical performance.

4. Conclusions

We here attempt to dope divalent cations of Zn^{2+}, Cu^{2+} and Ni^{2+} into Li_2FeSiO_4 via a sol–gel method. Zn^{2+} can be successfully doped into the lattice of Li_2FeSiO_4. Compared with the undoped Li_2FeSiO_4, the Zn doped sample exhibits better electrochemical performance in term of discharge capacity, electrochemical reversibility and electrode polarization. These improvements can be attributed to the improved lithium diffusion capability. However, Cu and NiO impurities are formed in the Cu- and Ni-containing samples, respectively, causing poorer electrochemical performance.

Acknowledgements

This work is supported by the National Natural Science Foundation of China (No. 50902041), Foundation for University Key Teacher by the Heilongjiang Ministry of Education (No. 1155G28), Postdoctoral Foundation of Heilongjiang Province (No. LBH-Q08057), Innovation Foundation of Harbin City (No. 2009RFQXG201) and Development Program for Outstanding Young Teachers in Harbin Normal University (No. KGB200805).

References

[1] A.K. Padhi, K.S. Nanjundaswamy, J.B. Goodenough, J. Electrochem. Soc. 144 (1997) 1188–1194.
[2] A.S. Prakash, P. Rozior, L. Dupont, H. Vezin, F. Sauvage, J.M. Tarascon, Chem. Mater. 18 (2006) 407–412.
[3] Y.H. Huang, H.B. Ren, S.Y. Yin, Y.H. Wang, Z.H. Peng, Y.H. Zhou, J. Power Sources 195 (2010) 610–613.
[4] R. Dominko, M. Bele, M. Gaberscek, A. Meden, M. Remskar, J. Jamnik, Electrochem. Commun. 8 (2006) 217–222.
[5] C. Lyness, B. Delobel, A.R. Armstrong, P.G. Bruce, Chem. Commun. 46 (2007) 4890–4892.
[6] R. Dominko, M. Bele, A. Kokalj, M. Gaberscek, J. Jamnik, J. Power Sources 174 (2007) 457–461.
[7] M.E. Arroyo-de Dompablo, R. Dominko, J.M. Gallardo-Amores, L. Dupont, G. Mali, H. Ehrenberg, J. Jamnik, E. Moran, Chem. Mater. 20 (2008) 5574–5584.
[8] M.E. Arroyo-de Dompablo, M. Armand, J.M. Tarascon, U. Amador, Electrochem. Commun. 8 (2006) 1292–1298.
[9] M.E. Arroyo-de Dompablo, U. Amador, J.M. Gallardo-Amores, E. Moran, H. Ehrenberg, L. Dupont, R. Dominko, J. Power Sources 189 (2009) 638–642.
[10] M. Nadherna, R. Dominko, D. Hanzel, J. Reiter, M. Gaberscek, J. Electrochem. Soc. 156 (2009) A619–A626.
[11] R. Dominko, D.E. Conte, D. Hanzel, M. Gaberscek, J. Jamnik, J. Power Sources 178 (2008) 842–847.
[12] R. Dominko, I. Arcon, A. Kodre, D. Hanzel, M. Gaberscek, J. Power Sources 189 (2009) 51–58.
[13] Z.L. Gong, Y.X. Li, Y. Yang, J. Power Sources 174 (2007) 524–527.
[14] A. Nyten, A. Abouimrane, M. Armand, T. Gustafsson, J.O. Thomas, Electrochem. Commun. 7 (2005) 156–160.
[15] A. Nyten, S. Kamali, L. Hanggstrom, T. Gustafsson, J.O. Thomas, J. Mater. Chem. 16 (2006) 2266–2272.
[16] A. Nyten, M. Stjerndahl, H. Rensmo, H. Siegbahn, M. Armand, T. Gustafsson, K. Edstrom, J.O. Thomas, J. Mater. Chem. 16 (2006) 3483–3488.
[17] A. Kokalj, R. Dominko, G. Mali, A. Meden, M. Gaberscek, J. Jamnik, Chem. Mater. 19 (2007) 3633–3640.
[18] R. Dominko, J. Power Sources 184 (2008) 462–468.
[19] R. Dominko, M. Bele, M. Gaberscek, M. Remskar, D. Hanzel, S. Pejovnik, J. Jamnik, J. Electrochem. Soc. 152 (2005) A607–A610.
[20] C. Delacourt, P. Poizot, S. Levasseur, C. Masquelier, Electrochem. Solid-State Lett. 9 (2006) A352–A355.
[21] Y.H. Chen, Y.M. Zhao, X.N. An, J.M. Liu, Y.Z. Dong, Electrochim. Acta 54 (2009) 5844–5850.
[22] R. Dominko, D. Conte, D. Hanzel, M. Gaberscek, J. Jamnik, J. Power Sources 178 (2008) 842–847.
[23] Z.L. Gong, Y.X. Li, Y. Yang, Electrochem. Solid-State Lett. 11 (2008) A60–A63.
[24] M. Wagemaker, B.L. Ellis, D. Lutzenkirchen-Hecht, F.M. Mulder, L.F. Nazar, Chem. Mater. 20 (2008) 6313–6315.
[25] S.Y. Chung, J.T. Bloking, Y.M. Chiang, Nature Mater. 1 (2002) 123–128.
[26] H. Xie, Z. Zhou, Electrochim. Acta 51 (2006) 2063–2067.
[27] M.R. Yang, W.H. Ke, J. Electrochem. Soc. 155 (2008) A729–A732.
[28] H.C. Shin, S.B. Park, H. Jang, K.Y. Chung, W.I. Cho, C.S. Kim, B.W. Cho, Electrochim. Acta 53 (2008) 7946–7951.
[29] Z.L. Gong, Y.X. Li, Y. Yang, Electrochem. Solid-State Lett. 9 (2006) A542–A544.
[30] L.M. Li, H.J. Guo, X.H. Li, Z.X. Wang, W.J. Peng, K.X. Xiang, X. Cao, J. Power Sources 189 (2009) 45–50.
[31] A.R. West, F.P. Glasser, J. Mater. Sci. 5 (1970) 557–565.
[32] C. Jousseaume, D. Vivien, A. Kahn-Harari, B.Z. Malkin, Opt. Mater. 24 (2003) 143–150.
[33] A.R. West, J. Appl. Electrochem. 3 (1973) 327–335.
[34] R. Yang, X.P. Song, M.S. Zhao, F. Wang, J. Alloys Compd. 468 (2009) 365–369.
[35] Y. Lu, J.C. Shi, Z.P. Guo, Q.S. Tong, W.J. Huang, B.Y. Li, J. Power Sources 194 (2009) 785–793.
[36] C. Deng, S. Zhang, S.Y. Yang, J. Alloys Compd. 487 (2009) L18–L23.
[37] H.M. Wu, J.P. Tu, X.T. Chen, Y. Li, X.B. Zhao, G.S. Cao, J. Electroanal. Chem. 586 (2006) 180–183.
[38] J. Barker, R.K.B. Gover, P. Burns, A. Bryan, J. Electrochem. Soc. 154 (2007) A307–A313.
[39] M. Gaberscek, J. Moskon, B. Erjavec, R. Dominko, J. Jamnik, Electrochem. Solid-State Lett. 11 (2008) A170–A174.
[40] Q. Cao, H.P. Zhang, G.J. Wang, Q. Xia, Y.P. Wu, H.Q. Wu, Electrochem. Commun. 9 (2007) 1228–1232.